Broadband Brightfield Inspection Enables Advanced Immersion Lithography Defect Detection

Catherine Perry-Sullivan, Erwan Le Roy, Steven R. Lange, Irfan Malik, Avinash Yerabaka, Adrian Wilson, Mark Shirey, Becky Pinto – KLA-Tencor Corporation

The materials employed in the immersion litho cell vary widely over different layers, products and fabs. A highly flexible brightfield inspector ensures maximum sensitivity over a broad range of immersion litho materials and defect types.

Immersion lithography is a key enabling technology for 65nm and 45nm device patterning. However, the introduction of a fluid between the wafer and scanner has led to new defectivity issues related to the intricate interactions between multiple process parameters – including the resist, topcoat, scanner and fluid.[1] While some immersion-specific defects, such as bubbles, have been successfully controlled or eliminated, immersion litho defect reduction remains a major challenge for chipmakers.[2,3,4,5] Long the standard for patterned wafer litho/photo-cell monitoring,[6,7] high-resolution broadband brightfield inspectors offer unique features that benefit immersion litho defect detection, monitoring and control. These features include a high numerical aperture (NA), a tunable illuminator covering DUV, UV and visible wavelengths, selectable optical apertures, and advanced automatic defect classification capability.

This paper presents experimental and theoretical data on several immersion litho defects and layers, showing how tunable broadband illumination and selectable optical apertures uniquely fulfill the resolution and noise suppression requirements for immersion litho defect detection. Several use cases demonstrate how broadband brightfield inspectors, with features such as automatic defect classification, help chipmakers solve immersion litho defect issues and successfully implement immersion lithography in production.

Immersion Lithography Defects: Simulation Studies

Inspection tool sensitivity can be described as being directly proportional to defect signal and inversely proportional to wafer noise. Maximizing the signal-to-noise ratio — or, the contrast between a defect and its surroundings — is necessary for the successful detection of critical immersion litho defects. For brightfield inspection, the optical properties of the defect and the surrounding material determine the relative contrast. These optical properties vary with differing materials and defect types, and are also a function of the illumination wavelength and optical apertures. As the combination of materials employed in the immersion litho cell varies widely over different layers, products and fabs, the use of a brightfield inspector with a tunable broadband illuminator and selectable apertures ensures maximum sensitivity over a broad range of immersion litho materials and defect types.

This section presents theoretical modeling data showing the wavelength and aperture dependence of two immersion litho defects. Additional simulation data is presented which demonstrates how small changes in material thicknesses in the resist stack can dramatically affect the optimal wavelength required for maximum defect sensitivity.

Simulation Model

Simulation studies were performed for two immersion litho defects – bridging and line thinning. Immersion litho bridging defects result in blocked pattern between adjacent lines and can be caused by water marks, stains or particles. Line

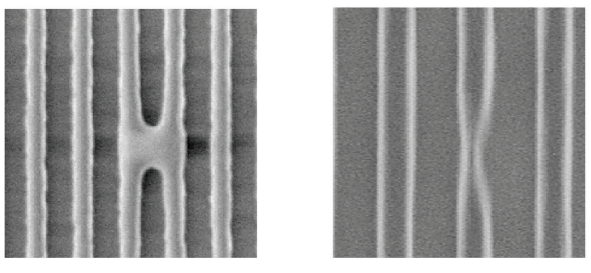

Figure 1: Example of bridging (left) and line thinning (right) defects.

thinning is a defect specific to immersion lithography which results in a deformation of the lines' critical dimension. Example SEM images of bridging and line thinning defects are shown in figure 1.

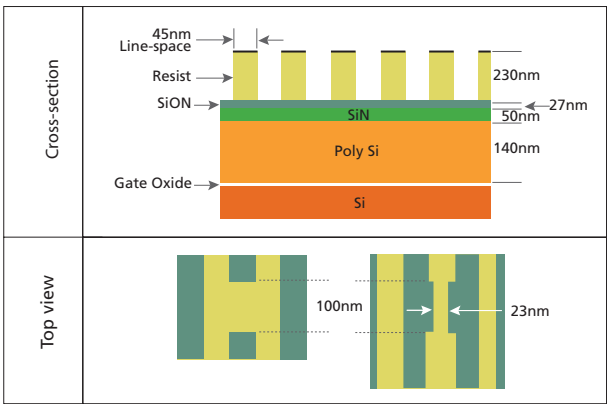

Figure 2: Cross-section and top view of the gate ADI layer used for the simulations. The pattern consists of 45nm resist lines on a SiON BARC. The bridging defect (bottom left) is 100nm long. The line thinning defect (bottom right) is 100nm long and 23nm wide.

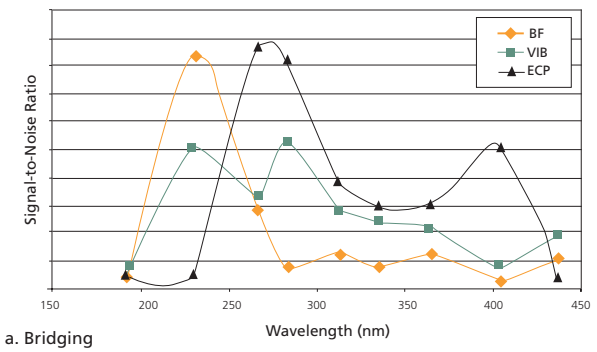

a. Bridging

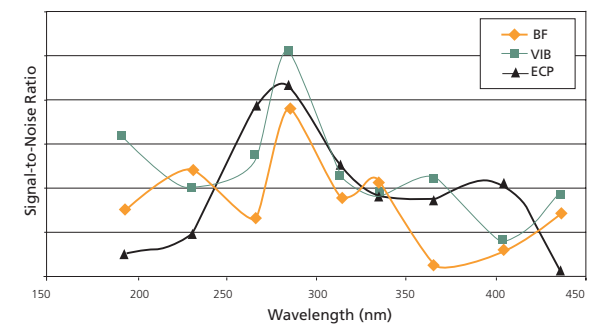

b. Line Thinning

Figure 3: Theoretical wavelength dependence of the signal-to-noise of a bridging defect (a) and a line thinning defect (b) on a 45nm gate ADI layer. Results for three different optical apertures are shown (BF, VIB and ECP). The optimal signal-to-noise depends on both the illumination wavelength and optical aperture. These data indicate that both defect types would exhibit sufficient signal-to-noise for simultaneous defect capture by using a DUV illumination source (250 – 300nm) with the ECP aperture.

A gate ADI process layer was used in the modeling studies. A cross-section and top view of this layer are shown in figure 2. The pattern consists of 45nm resist lines on a SiON bottom anti-reflective coating (BARC). The bridging defect used in the simulations is 100nm long, while the line thinning defect is 100nm long and 23nm wide. Included in the model were two noise sources: line edge roughness and color variation due to resist thickness variations.

For both defects, the theoretical signal-to-noise ratio was calculated. This was done by first calculating the defect's gray level signal, that is, the difference in gray level between an image with the defect and an image without the defect. Similarly, the noise gray level value was found by taking the difference in gray level between an image with line edge roughness and color variation noise and an image without any noise sources. The signal-to-noise was then calculated by taking the ratio of the defect gray level signal and the noise gray level value. The simulations looked at both the wavelength dependence of the signal-to-noise, and the effect of different optical apertures on the signal-to-noise ratio.

Modeling Results

The theoretical wavelength dependence of the signal-to-noise of the bridging and line thinning defects is shown in figure 3. Simulations were performed using three different optical apertures: (1) BF, a standard brightfield aperture; (2) ECP (Edge Contrast Plus), an illumination technique which allows high-angle illumination; and, (3) VIB (Varied Illumination Brightfield), an illumination technique which allows low-angle illumination.

Figure 3a shows that the optimal wavelength for the bridging defect depends strongly on the aperture utilized. The highest signal-to-noise ratios are obtained using either the ECP aperture with an illumination spectrum near 270nm, or the brightfield aperture with an illumination spectrum near 230nm. The wavelength dependence of the signal-to-noise for the line thinning defect (Figure 3b) is similar for the three apertures, with the highest signal-to-noise obtained using the VIB aperture with an illumination spectrum near 290nm. These simulation data indicate that for this 45nm gate ADI immersion litho layer with line edge roughness and color noise, sufficient signal-to-noise for simultaneous detection of both defects would be obtained using the ECP aperture with a DUV illumination source covering 250-300nm wavelengths. While these modeling data suggest that a brightfield inspector with a tunable broadband illumination source and selectable apertures is necessary for detection of different defect types on an immersion litho layer, the following section demonstrates that these brightfield attributes are required to address the optical property variations exhibited by different resist stacks.

Materials Wavelength Dependence

The compositions and thicknesses of BARC, top anti-reflective coating (TARC), resist and other materials used in immersion lithography can vary dramatically over different process levels, products and fabs. These varying resist stacks exhibit different physical and optical properties. Modeling data from two

different resist/BARC stacks demonstrate how small changes in stack composition can result in widely varying optical properties.[8] These simulations were performed for a bridging defect on a 90nm line-space array. Both material stacks were based on fab prescriptions for 193nm litho and cross-sections are shown in figure 4. Stack A consisted of 230nm of resist on 27nm of a SiON BARC, while Stack B had 150nm of resist on 45nm of BARC. The theoretical wavelength dependence of the brightfield gray-level signal for the bridging defect on these two stacks is shown in figure 4. The optimal wavelength for detection of the bridging defect depends strongly on the resist/BARC stack composition. The highest defect signal for Stack A is obtained with visible light in the 440-500nm range, while the highest defect signal for Stack B is obtained with DUV light in the 200-300nm range. Future modeling studies will include a closer investigation of the wavelength dependence of specific immersion litho stacks and materials at smaller design rules.

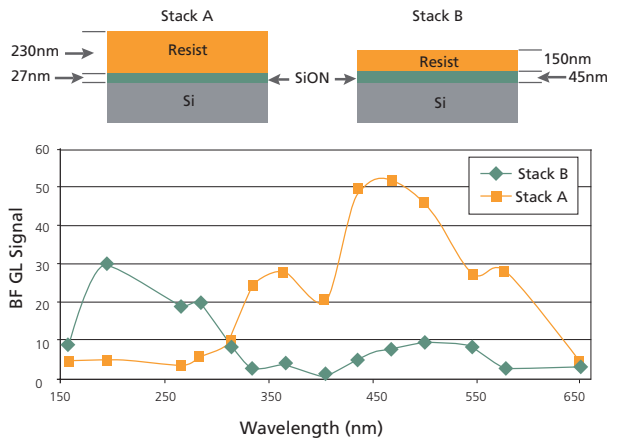

Figure 4: Modeling data shows the wavelength dependence of the brightfield gray-level signal of a bridging defect on a 90nm line-space array for two different litho stacks. Stack A (orange line; 27nm of BARC topped with 230nm of resist) exhibits the strongest defect signal in the visible wavelength range (440-500nm), while Stack B (green line; 45nm of BARC topped with 150nm of resist) has the strongest defect signal in the DUV wavelength range (200-300nm).

Immersion Lithography Defects: Experimental Data

Experimental signal-to-noise ratios from defects on two immersion litho wafers are presented below. Results from one wafer focus on the wavelength dependence of the signal-to-noise ratios, while data from the second wafer examine the effect of different optical apertures on the signal-to-noise.

Metal ADI Wafer

The following studies were done on a metal ADI wafer patterned using an immersion scanner. This is a flash device with ~55nm design rule. The experimental data on this wafer were collected using a broadband brightfield inspector with a tunable illumination source and selectable apertures. These data include signal-to-noise ratios calculated from TDI sensor difference images. A difference image highlights the signal and noise characteristics of a defect and is the image that results from subtracting the raw sensor image of a reference die from the raw sensor image of a defective die. Figure 5 shows examples of TDI sensor difference images for a bridging defect on this wafer. These difference images were taken using three

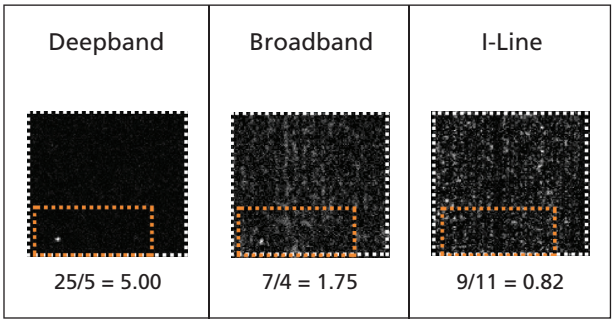

Figure 5: TDI sensor difference images of a bridging immersion litho defect from a ~55nm metal ADI layer. Images were collected with a 2800 broadband brightfield inspector using different wavelength ranges. These images show that deepband illumination – covering a range of DUV wavelengths – is best for suppressing noise and maximizing the defect's signal-to-noise ratio.

different illumination wavelength ranges — deepband, broadband and I-line — with the standard brightfield aperture. Deepband covers a range of DUV wavelengths, broadband covers DUV and UV wavelengths, and I-line centers around 365nm UV wavelength. The number under each image is the signal-to-noise ratio of the defect, calculated from the difference image by measuring the signal of the defect and the noise of the surrounding pattern area. These data show deepband as the best illumination source for noise suppression and defect detection. Qualitatively, the area surrounding the defect

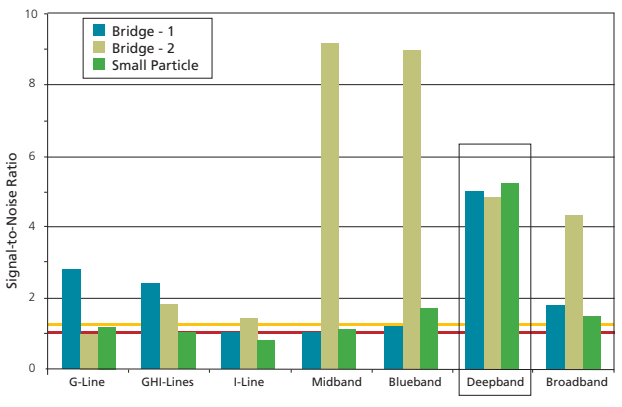

Figure 6: Signal-to-noise ratios of three immersion litho defects (two bridges and one small particle) on a ~55nm metal ADI wafer calculated from TDI sensor difference images collected using a 2800 broadband brightfield inspector using different wavelength bands and the standard brightfield aperture. While a defect will not be detected unless its signal-to-noise value is above 1.0 (red horizontal line), it is sufficiently above the noise floor for consistent detection when its signal-to-noise value is above 1.3 (yellow horizontal line). These data show that deepband illumination – covering a range of DUV wavelengths – is best for maximizing the signal-to-noise ratio for all three defects.

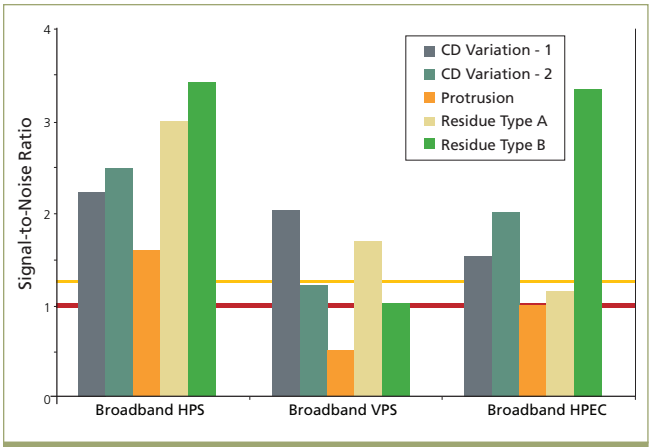

Figure 7: Signal-to-noise ratios of five immersion litho defects from a ~45nm PCM wafer calculated from TDI sensor difference images. A 2800 broadband brightfield inspector using broadband DUV illumination and three different apertures was used to collect the images. The yellow horizontal line indicates the signal-to-noise value (1.3) that is sufficiently above the noise floor for consistent defect detection, while the red horizontal line indicates the absolute minimum value (1.0) necessary for detection. These data show that the HPS aperture – which suppresses horizontal pattern edges – is best for maximizing the signal-to-noise ratio for all five defects.

appears 'quiet,' while quantitatively, the highest signal-to-noise ratio is obtained with deepband illumination.

Figure 6 shows the signal-to-noise ratios for three different immersion litho defects from this wafer, collected using seven different illumination bands with the standard brightfield aperture. Deepband, blueband and midband all cover different DUV wavelength ranges while broadband covers both DUV and UV wavelengths. G-line centers around 436nm visible wavelength, I-line centers on 365nm UV wavelength, and GHI-line covers a range of UV and visible wavelengths. These data show that G-line and I-line illuminations provide poor signal-to-noise for two of the three defects. Likewise, while the signal-to-noise ratio is very high for one bridging defect using midband and blueband, these illumination ranges result in marginal signal-to-noise ratios for the other two defects. Broadband illumination provides adequate signal-to-noise for all three defects. However, deepband proves to be the best illumination source for noise suppression and defect detection on this particular wafer as all three defects have high signal-to-noise ratios. These data demonstrate how the signal-to-noise ratios are strongly affected by the wavelength range selected for illumination.

PCM Wafer

These experimental data were collected on a PCM (photo-cell monitor; resist on silicon) wafer patterned using an immersion scanner. This is a flash device with ~45nm design rule. The data on this wafer were collected using a broadband brightfield inspector with a tunable illumination source and selectable apertures, and include signal-to-noise ratios calculated from TDI sensor difference images for five different defects. The immersion defect types studied include: CD variation (widening of the line), protrusion, and two types of residues. These data were collected using broadband DUV illumination with three different apertures. The apertures utilized include two which suppress horizontal or vertical pattern edges (HPS and VPS), and HPEC (Higher Performance Edge Contrast) which is an optical technique that allows darkfield imaging. The signal-to-noise ratios are shown in figure 7.

These data clearly show that the HPS aperture provides the highest signal-to-noise ratio for all the immersion litho defects on this particular wafer, and is the best aperture to utilize for maximum defect sensitivity. While the experimental data in the previous section demonstrated the value of a tunable illumination source for minimizing noise and maximizing defect detection, these data demonstrate how different apertures can affect the resulting signal-to-noise ratios. In order to obtain maximum defect sensitivity on a variety of immersion litho layers and defects, a brightfield inspector requires the flexibility provided by both a tunable broadband illumination source and selectable apertures.

Immersion Lithography Defectivity: Use Cases

Two of the following use cases compare the defect detection capabilities of DUV broadband brightfield and UV broadband brightfield inspectors on immersion litho wafers. The third use case focuses on the value of automatic defect classification for immersion litho defect monitoring.

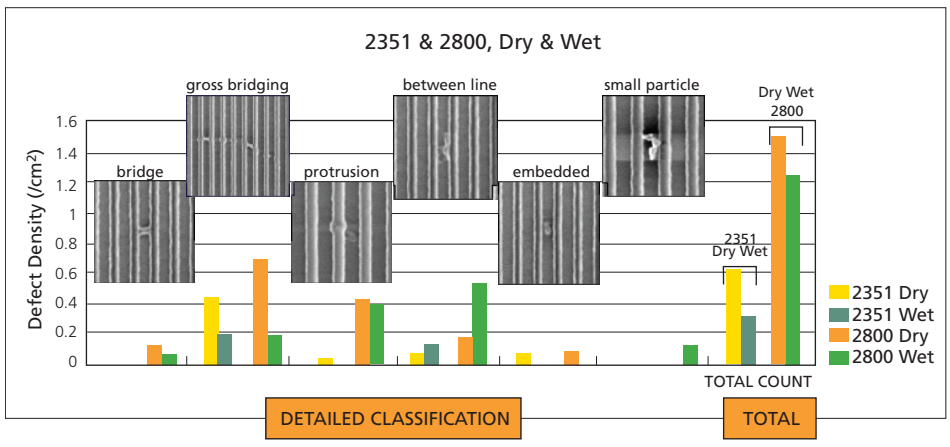

Figure 8: Defect detection comparison between the 2800 DUV broadband brightfield inspector and the 2351 UV broadband brightfield inspector on a 90nm array immersion litho wafer.[9] The 2800 shows 2x to 4x higher defect capture and unique capture of bridging defects.

Scanner Qualification

One scanner manufacturer recently studied defectivity levels obtained with its immersion scanner under different process conditions.[9] As part of these studies, the immersion defect detection capability of a DUV broadband brightfield inspector was compared with a UV broadband brightfield inspector on 90nm array devices. While no defects specific to the immersion process were detected, the DUV broadband brightfield inspector did detect unique bridging defects and provided 2x (dry) to 4x (wet) higher defect capture than the UV broadband brightfield inspector (Figure 8).

The DUV broadband brightfield inspector also captured 45nm defects – a 2x improvement in the minimum defect size detected by the UV broadband brightfield inspector. The improved sensitivity and defect capture demonstrated by the DUV broadband brightfield inspector prove its necessity for defect detection and control on immersion litho layers.

Immersion Lithography Integration

One semiconductor manufacturer implemented a comprehensive defect monitoring strategy involving both unpatterned and patterned wafer inspection in order to accelerate immersion lithography development and production integration.[10] As part of its investigation of patterned wafer inspectors, it compared the immersion defect detection performance of a DUV broadband brightfield inspector with a UV broadband brightfield inspector on resist imaging stacks on bare silicon. The resulting Pareto and example images of defect types are shown in figure 9.

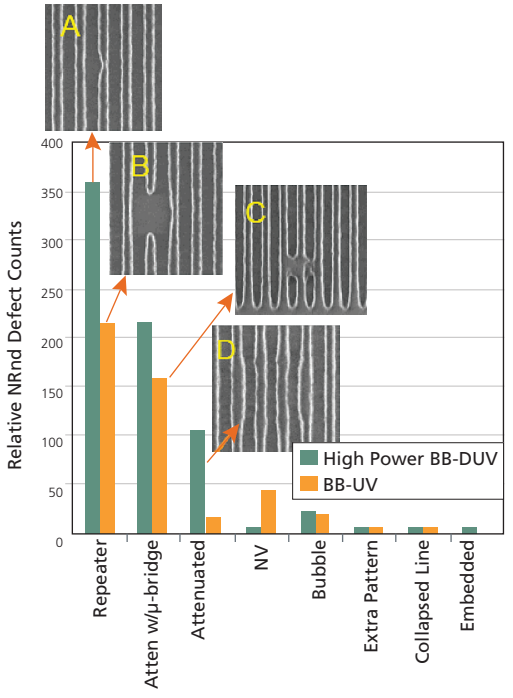

Figure 9: Defect Pareto comparing the immersion litho defect detection performance of the 2800 DUV broadband brightfield inspector and the 2365 UV broadband brightfield inspector on a resist imaging stack on bare silicon.[10] The 2800 shows much higher defect capture, and uniquely captures defect types A (protrusion repeater) and D (attenuated).

This Pareto shows that the DUV broadband brightfield inspector provided higher capture of all defect types when compared to the UV broadband brightfield inspector. Though they are grouped with similar defect types in the Pareto, the chipmaker indicated that protrusion repeaters (defect type A in figure 9) and attenuated defects (type D) were uniquely captured by the DUV broadband brightfield inspector. The chipmaker considered the attenuated defect to be a key immersion litho defect type. Overall, this chipmaker found that the DUV broadband brightfield inspector provided higher total defect capture, and was better at capturing smaller and more subtle immersion litho defects.

These results show that the DUV broadband brightfield inspector is a key tool for the identification and characterization of immersion-specific defects. For this chipmaker, the implementation of a comprehensive defect monitoring strategy, including a DUV broadband brightfield inspector, resulted in the successful production of 45nm test lots in the immersion cluster at defect densities equivalent to those obtained with dry lithography.

Automatic Defect Classification

As immersion lithography is integrated in production, chipmakers must quickly isolate and identify specific defectivity issues. As part of this process, it is important that an inspector not only capture the critical immersion litho defects, but also provide automated review sample shaping to filter nuisance defects and bin defects of interest. Integrated automatic defect classification allows chipmakers to work on process fixes in a logical order – first addressing the most critical immersion litho defect types, then tackling defects with less yield impact.

For one immersion litho engineering team, it was difficult to diagnose and fix critical immersion litho process problems based on the high total number of defects reported on each wafer. The value of automated defect classification was demonstrated using a DUV broadband brightfield inspector which utilizes proprietary information from the detection algorithms and optics to bin defects by specific attributes.

This automated binning capability reduced time to critical information by removing line roughness nuisance defects from the defect population and by binning the remaining defects by type – particularly, separating protrusions from other real defects such as bridging and stringers (Figure 10). This binning capability allowed the litho engineer to diagnose immersion process problems associated with major bridges and stringers first, before moving on to process issues related to the more subtle protrusion defects. Utilizing an inspector with automatic defect classification capability reduces time to meaningful results and assures that resources are allocated towards fixing the most significant immersion litho yield issues.

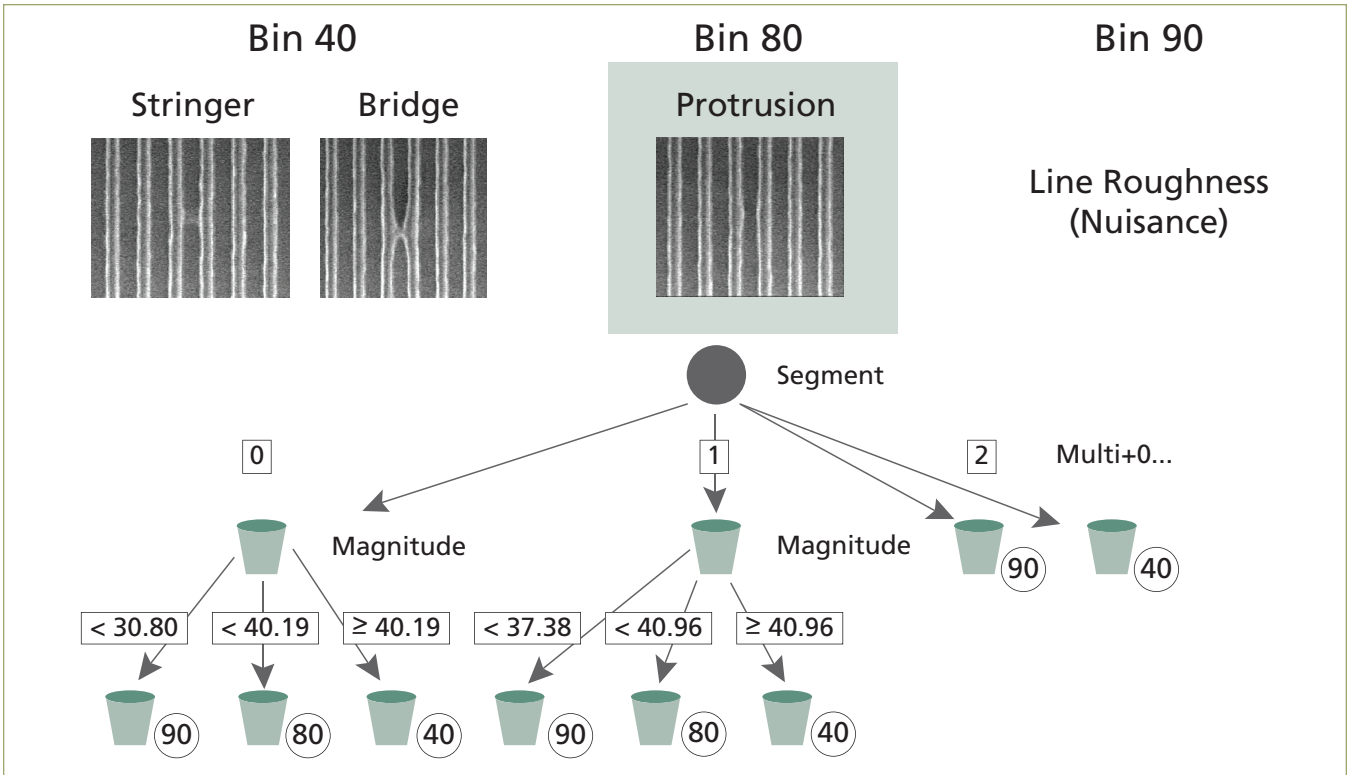

Figure 10: The 2800 DUV broadband brightfield inspector provides advanced automatic defect classification capability with inline Defect Organizer™ (iDO™). iDO utilizes proprietary information to bin defects by specific attributes and includes an intuitive graphic interface. In this example, iDO removed line roughness nuisance from the defect population, and binned the remaining defects by type. This allowed the immersion litho engineers to focus on yield issues related to the stringer and bridging defect types (bin 40) before moving on to the less-critical protrusion defects (bin 80).

Conclusion

As immersion scanners are integrated into 65nm and 45nm production, chipmakers face new and complex challenges associated with immersion litho defectivity. As the experimental and theoretical data in this paper demonstrated, a broadband brightfield inspector with a tunable illumination source and selectable apertures is required for reducing common litho noise sources, maximizing the contrast of a range of immersion litho defects, and handling the optical property variations resulting from different stack compositions and materials. Future modeling studies will further explore the wavelength and aperture dependence of varying immersion resist stacks on ≤45nm design rule devices.

Use cases demonstrated the immersion litho detection capability of a DUV broadband brightfield inspector for both scanner qualification and immersion litho production integration. Additionally, the use of automatic defect classification reduced time to results and focused resources on the most critical immersion litho defect issues.

By providing the flexibility required to maximize defect sensitivity on a variety of immersion litho layers and materials, broadband brightfield inspectors are well positioned to address the immersion litho defectivity issues associated with production integration.

References

1. I. Malik and B. Pinto, "Immersion Changes Litho Cluster Qualification," Semiconductor International, September 2006.

2. L. Peters, "Defectivity Issues Drive Immersion Lithography," Semiconductor International, April 2006.

3. S. Warrick, D. Cruau, A. Mauri, V. Farys and S. Gaugiran, "A defectivity checkpoint for immersion lithography," Microlithography World, August 2006.

4. I. Malik and S. Nag, "Defectivity Challenges in Immersion Lithography for sub 90nm Technologies," Lithography Users Forum, February 2006.

5. M. David Levenson, "Immersion Symposium report: Industry optimistic about commercial success," Solid State Technology, October 2006.

6. S. Ashkenaz, I. Peterson, P. Marella, M. Merrill, L. Cheung, A. Sethuraman, T. DiBiase, M. Stoller, and L. Breaux, "Defect Management for 300mm and 130nm Technologies, Part 2: Effective Defect Management in the Lithography Cell," Yield Management Solutions, Fall 2001.

7. I. Peterson, L. Breaux, A. Cross and M. von den Hoff, "Successful demonstration of a comprehensive lithography defect monitoring strategy," SPIE Vol. 5041, pp. 70 – 81, 2003.

8. S. Lange, B. Pinto and J. Fernandez, "Advantages of Broadband Illumination for Critical Defect Capture at the 65nm Node and Below," Electronics Journal (Japanese), July 2006.

9. K. Nakano, S. Nagaoka, S. Owa, T. Yamamoto and I. Malik, "Immersion defectivity analysis using volume production immersion exposure tool," 3rd International Symposium on Immersion Lithography, October 2006.

10. C. Robinson, D. Corliss, S. Ramaswamy, "Immersion Lithography Defect Learning," 3rd International Symposium on Immersion Lithography, October 2006.